

Molecular Dynamics Simulation of Xenon Diffusion in UO₂ Nanocrystals

Kichigina N.V., Nekrasov K.A., Kupryazhkin A.Ya.

 Department of Technical Physics
 Ural Federal University
 Yekaterinburg, Russia
 k.a.nekrasov@urfu.ru

Gupta S.K.

 Department of Physics
 St. Xavier's College
 Ahmedabad, India
 sanjeev.gupta@sxca.edu.in

Abstract—Diffusion of individual xenon atoms in the bulk of UO₂ nanocrystals with free surface is studied using the molecular dynamics approach. Two sets of the pair potentials of interaction of the Xe atom with uranium and oxygen ions are considered. For both sets, interstitial migration is observed, as well as the atom trapping in the uranium sites. However, the quantitative characteristics of these processes are found to be very different. The coefficients of Xe interstitial migration are obtained in the temperature range from 2400 K up to the melting point of the model crystals. The corresponding activation energies have the values of 2.5 eV and 2.2 eV depending on the interaction potentials. The results of the simulation are compared with the experimental data.

Keywords—uranium dioxide; radiogenic xenon; diffusion; molecular dynamics; interaction potentials

I. INTRODUCTION

Accumulation of radiogenic xenon in nuclear fuel causes swelling of the material and degrades its operational characteristics. Release of the gas from the fuel tablets increases the pressure under the fuel rod shell, which can lead to cracking of the shell. Transport of xenon in the oxide fuels such as UO₂ can be studied using the molecular dynamics simulation. This approach is particularly important since experimental studies of the irradiated fuel are very complicated.

Until recently, molecular dynamic simulation of the system xenon – oxide fuel (mainly, UO₂) was limited to studying the state of xenon bubbles, the process of resolution of Xe atoms from a bubble to the crystal lattice [1-2] and xenon diffusion along the grain boundaries [3]. Characteristics of the state and transport of xenon atoms in the bulk of the crystal lattice were determined by static methods (for example [4-5]). The limited dynamic modeling was due to the low mobility of the xenon atom in the crystal lattice.

In the present work, the method of molecular dynamics is used to simulate migration of individual xenon atoms in nano-sized crystals of uranium dioxide that have free surface, being isolated in vacuum. The computational power required for the modeling is provided by parallelizing the crucial calculations on the CUDA-based graphics processors, such as GK110 and GP102.

II. THE SIMULATION PROCEDURE

A. The Model System

The systems simulated in this work were UO₂ nanocrystals of octahedral shape isolated in vacuum. Thus, the crystals had free surface. Most of the crystals consisted of 5460 ions, which corresponds to the linear dimensions of about 4 nm (at higher temperatures, the size was increased up to 65 000 particles). This comparatively small size was used to increase the intrinsic time of evolution of the system, which reached $1.5 \cdot 10^{-6}$ s. Such long evolution times were necessary in connection with the low mobility of the xenon atoms trapped in the uranium sites.

The single xenon atom was initially placed in one of the central interstitial positions. The computational experiments tracked migration of this atom until its release at the surface. The free surface also acted as the source of the vacancies to accommodate the dissolved Xe atom.

The initial velocities of the intrinsic ions and Xe atom were generated in accordance with the Maxwellian distribution of the components at required temperature T . A linear congruent generator was used to obtain standard random numbers γ_i , to which the Box-Muller transform [6] was applied. As a result, the components of velocity vector v_j were calculated from formulas:

$$v_j = (2kT \cdot |\ln(\gamma_{1,j})| / m)^{1/2} \cdot \cos(2\pi\gamma_{2,j}), \quad (1)$$

where index j stands for the x , y or z -components of vector; m is the particle mass and k is the Boltzmann's constant.

To control the temperature during a computational experiment, the Berendsen thermostat [7] was applied.

B. The Interaction Potentials

A number of sets of *ab initio* interaction of potentials for the Xe – UO₂ system have been suggested. One such set was calculated using the relativistic Hartree-Fock method [4], and others were fitted to data obtained from the density functional theory (DFT) calculations [8–10]. Here, the authors restricted their attention to the potentials [4] and [10]. The former set was chosen because it was calculated directly and

independently of the model of the UO_2 crystal. The latter set is one of the most recent. Thus, two sets of *ab initio* interaction of potentials for the Xe–uranium and Xe–oxygen pairs were used:

- The relativistic Hartree-Fock potentials were proposed by R.A. Jackson and C.R.A. Catlow in 1985 [4]. Hereinafter, the authors refer to these potentials as Potentials I.

- The potentials that were fitted to the calculations of density functional theory with the Hubbard U correction (DFT + U) by A.E. Thompson, B. Meredig and C. Wolverton in [10] (2014). The authors used a method called iterative potential refinement to fit the potentials to energy, forces, and stresses obtained from static and dynamic DFT calculations for the xenon atom in the UO_2 crystal. Further on, this set is considered as Potentials II.

It is important to note that the energies of solution of the xenon atom in the interstitial positions, vacancies and vacancy clusters calculated by means of Potentials II are considerably lower than for other potentials, including Potentials I.

There is a large selection of the potential set for modeling the interaction of uranium dioxide intrinsic ions. In this work, the potentials MOX-07 [11] were chosen to use them in conjunction with Potentials I, based on the comparison of the potentials in the works [11-13]. The advantage of the MOX-07 set is a relatively good reproduction of the UO_2 lattice constant of at high temperatures, the energies of formation of the intrinsic point defects and the melting point. On the other hand, the procedure for obtaining Potentials II implied their use with the intrinsic UO_2 potentials developed by Basak et al. [14]. Therefore, potentials [14] (designated below as Basak-2003) were used together with Potentials II.

For the calculations, all the interaction potentials $U(R)$ were represented in the form:

$$U(R) = K_E \cdot q_1 q_2 / R + A e^{-BR} - C/R^6 + \varepsilon \cdot (e^{-2\beta(R-Rm)} - 2e^{-\beta(R-Rm)}), \quad (2)$$

where R is the distance between the centers of the interacting particles, K_E is the Coulomb law constant, q_1 and q_2 are the charges of the particles, and other constants are parameters of the potential. The values of the parameters are listed in Tables I–IV. In form (2), potential $U(R)$ takes into account the Coulomb interaction of the charged particles such as oxygen and uranium ions, the repulsion of overlapping electron shells and the dispersive attraction. The last term of function (2) is the Morse potential [15] which emulates the chemical bonding of neighboring ions.

Some of the parameters in (2) were not used for particular pairs. Most of the null parameters are omitted in Tables I–IV.

TABLE I. THE PARAMETERS OF POTENTIALS I [4]

Parameter	Interacting particles	
	Xe-U	Xe-O
A, eV	2788.45	1471.18
B, 10^{10} m^{-1}	-2.41404	-2.64497

TABLE II. THE PARAMETERS OF POTENTIALS II [10]

Parameter	Interacting particles	
	Xe-U	Xe-O
A, eV	6607300	95913.0
B, 10^{10} m^{-1}	-5.61798	-4.76190

TABLE III. THE PARAMETERS OF POTENTIALS MOX-07 [11]

Parameter	Interacting particles		
	O-O	O-U	U-U
$K_E \cdot q_1 q_2$, $\text{eV} \cdot 10^{-10} \text{ m}$	39.5262	-79.0524	158.105
A, eV	50211.7	873.107	0.0
B, 10^{10} m^{-1}	-5.52001	-2.78385	0.0
C, $\text{eV} \cdot 10^{-60} \text{ m}$	74.7961	0.0	0.0

TABLE IV. THE PARAMETERS OF POTENTIALS BASAK-2003 [14]

Parameter	Interacting particles		
	O-O	O-U	U-U
$K_E \cdot q_1 q_2$, $\text{eV} \cdot 10^{-10} \text{ m}$	34.5594	-69.1188	138.238
A, eV	1633.01	693.649	0.0
B, 10^{10} m^{-1}	-3.05792	-3.05792	0.0
C, $\text{eV} \cdot 10^{-60} \text{ m}$	3.94879	0.0	0.0
ε , eV	0.57719	0.0	0.0
β , 10^{10} m^{-1}	1.65	0.0	0.0
Rm, 10^{-10} m	2.369	0.0	0.0

C. Equations of Motion Integration Scheme

The coordinates of the particles, evolved with time, are subject to the Newton's equations of motion and the leapfrog integration scheme:

$$\mathbf{x}_i(t + \Delta t) = \mathbf{x}_i(t) + \mathbf{v}_i(t + \Delta t/2) \cdot \Delta t, \quad (3)$$

$$\mathbf{v}_i(t + \Delta t/2) = \mathbf{v}_i(t - \Delta t/2) + (\mathbf{F}_i(t) / m_i) \cdot \Delta t, \quad (4)$$

where i was the particle index, t was the current time, $\Delta t = 3 \cdot 10^{-15} \text{ s}$ was the time integration step, $\mathbf{x}_i(t)$, $\mathbf{v}_i(t)$ and $\mathbf{F}_i(t)$ were the vectors of coordinates, velocities of the particle and the resulting force acting on it, m_i was the particle mass.

III. XENON DIFFUSION COEFFICIENTS

A. General Considerations

In the modeling, using both Potentials I and Potentials II, interstitial migration of xenon, trapping of the atoms in uranium sites, as well as their subsequently released atoms from the sites to interstitial positions were observed. Interstitial migration was characterized by relatively high

mobility of the atoms, whereas in uranium sites they were practically motionless.

Let us note that the capture of the xenon atom by a site of the uranium sublattice did not require pre-existence of the vacancy in it. The uranium ion was displaced by the xenon atom to the surface. Occupying the uranium site, the xenon atom could attach oxygen vacancies, since their effective charges against the lattice are opposite. However, this process was not investigated in the present work.

To measure diffusion coefficient D of xenon in the computational experiments, the time dependences of the square displacement of atom $a^2(t)$ were considered. The displacements were calculated with respect to the initial interstitial position of the atom or the equilibrium position in the uranium sites.

In the case of interstitial migration, it was possible to obtain fairly accurate dependencies of the mean square displacement of Xe atoms on time. Being averaged over a sufficient number of the computational experiments, these dependencies obeyed the well-known Einstein relation:

$$\langle a^2(t) \rangle = 6 \cdot D \cdot t. \quad (5)$$

It was necessary to have at least 20 measurements to obtain a qualitative averaging.

B. Simulation using Potentials I

The systems, simulated using Potentials I, were characterized by the longest periods of immobility of xenon atoms in the uranium sites. The regions of interstitial migration were much shorter, but also consisted of separate "steps" corresponding to quasi-equilibrium states of the atom in a succession of the adjacent interstitial positions.

Dependence $a^2(t)$ for an individual atom is illustrated in Fig. 1 and 2. Fig. 1 demonstrates the complete process of release of the atom from a nanocrystal. Fig. 2 shows an enlarged fragment of the graph in Figure 1 that lies within the dashed lines.

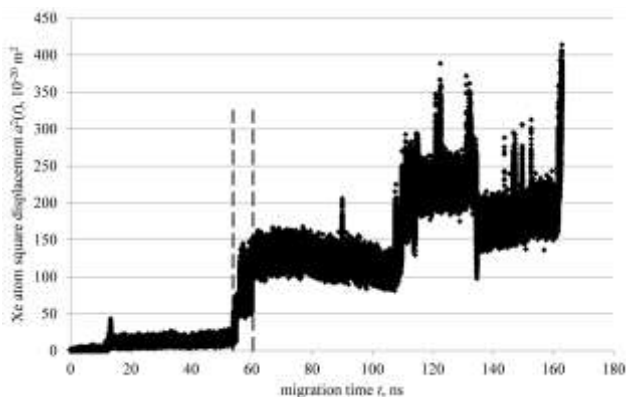


Fig. 1. The square of a xenon atom displacement in UO_2 at $T = 3025$ K during complete migration time span. Potentials I are used.

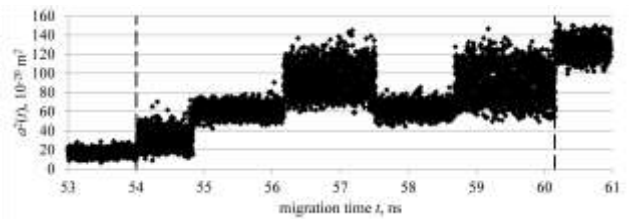


Fig. 2. The square of a xenon atom displacement in UO_2 at $T = 3025$ K. A region of interstitial migration. Potentials I are used.

For each of the regions of interstitial migration, the squares of the displacement of the atom were calculated relative to the equilibrium vacancy position where the atom was located before the beginning of the region. The mean square displacements were averaged over all such regions in all the computational experiments at the same temperature. An example of the resulting $\langle a^2(t) \rangle$ curve (corresponding to $T = 3025$ K) is shown in Fig. 3.

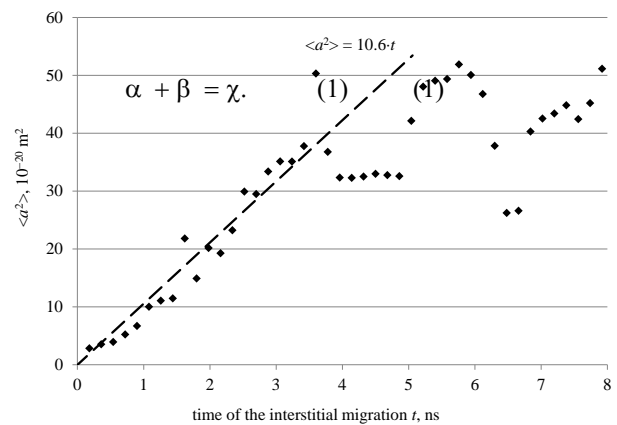


Fig. 3. The mean square of the atom displacement during the interstitial migration at $T = 3025$ K. Potentials I are used.

The curve in Fig. 3 has two regions where the mean square displacement behaves differently. The linear part of the dependence at small times corresponds to the Einstein relation (5). For large times, the linear growth of the mean square displacement is discontinued, since the displacement of atoms is limited by the size of the nanocrystal.

Using the simulation results and the relation (5), the authors were able to obtain the coefficients of the xenon interstitial diffusion in the temperature range from 2840 K to 3025 K. At lower temperatures, the xenon atoms remained trapped in the vacancies during the entire simulation time, whereas at higher temperatures, the model nanocrystals melted.

The dependence of the calculated diffusion coefficient on temperature is shown in Fig. 4. The Arrhenius coordinates are used to obtain the activation energy of diffusion in the form of the slope of straight line $\ln(D) = f(1/kT)$. The activation energy given by the graph is $E_D[I] = (2.5 \pm 0.7)$ eV.

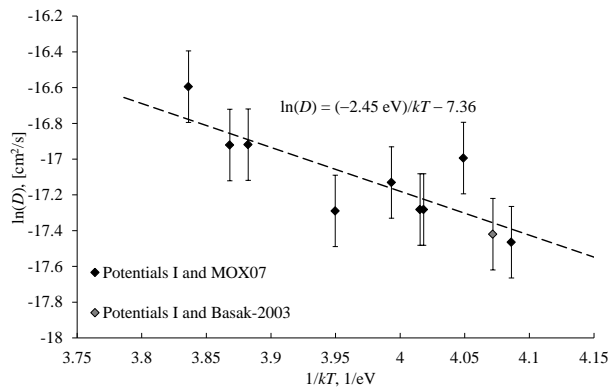


Fig. 4. The xenon diffusion coefficients obtained for Potentials I.

One of the points in Fig. 4 corresponds to using the Basak-2003 potentials [13] to simulate the UO_2 crystal in conjunction with Potentials I. The position of this point does not differ from others, which suggests that there is no fundamental influence of the choice between the Basak-2003 and MOX-07 potentials on the results of the simulation.

C. Simulation using Potentials II

In comparison with Potentials I, Potentials II in the present study were characterized by essentially shorter times of the release of xenon atoms from the uranium sites into the interstitial positions. With the use of Potentials I, the release times reached hundreds of nanoseconds, even at temperatures close to the melting point (Fig. 1). In the case of using Potentials II, the release time of the xenon atoms from the cation sites was reduced to several nanoseconds even for relatively low temperatures, as shown in Fig. 5.

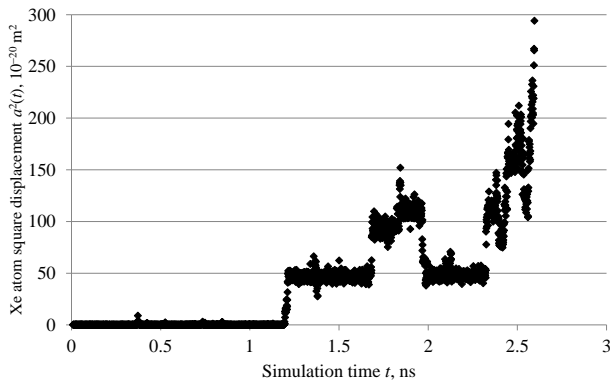


Fig. 5. The square of a xenon atom displacement in UO_2 at $T = 2400$ K during the complete time span until release of the atom from the nanocrystal. Potentials II are used.

The processing of the interstitial migration yielded dependences $\langle a^2(t) \rangle$ similar to the one shown in Fig. 3, and the Einstein relation was utilized to obtain the diffusion coefficients. The temperature dependence of the calculated diffusion coefficient is shown in Fig. 6 using the Arrhenius coordinates. The activation energy obtained from the straight line, approximating the data, is $E_D[\text{II}] = (2.2 \pm 0.2)$ eV.

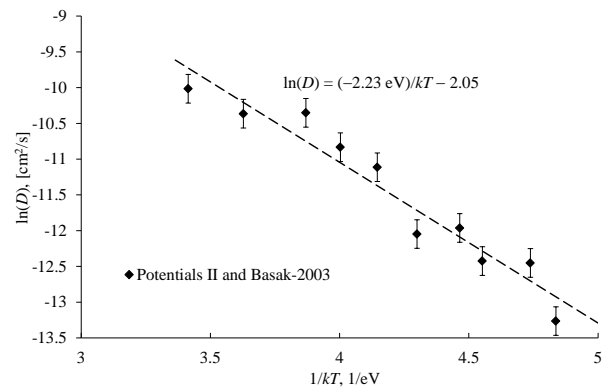


Fig. 6. The xenon diffusion coefficients obtained for Potentials II.

It is interesting that $E_D[\text{II}]$ is close to $E_D[\text{I}]$, despite the fundamental difference in the times of the release of the atom from the uranium sites that must correspond to a large difference in the activation energies of the release.

At the same time, the values of the interstitial diffusion coefficients obtained using Potentials II (D_{II}) are significantly higher than those, corresponding to Potentials I (D_{I}). The values of D_{I} lie in range $(2 \div 6) \cdot 10^{-8}$ cm^2/s for temperatures from 2840 K to 3025 K, whereas coefficients D_{II} increase from $1.5 \cdot 10^{-6}$ to $4.5 \cdot 10^{-5}$ cm^2/s as the temperature changes from 2400 K to 3400 K.

A superionic transition (disordering of the anion sublattice that resembles melting) occurs in the uranium dioxide crystal at the temperature of ~ 2700 K. This transition is reproduced by both the MOX-07 and the Basak-2003 potentials. The presence of the superionic transition could affect the temperature dependence of the interstitial diffusion coefficient calculated with Potentials II (Fig. 6). No clear evidence of such influence was found. This may be because xenon transport is predominantly controlled by the state of the cation sublattice.

When Potentials II were used, there was the possibility of a rough estimate of the effective activation energy of xenon diffusion, taking into account both interstitial diffusion and trapping of the atoms in the uranium sites. To carry out this task, the authors averaged the square displacements $a^2(t)$ over the entire migration process not separating the regions of interstitial migration and the trapping. This procedure yielded meaningful results for the high temperatures above 3000 K (namely, $T_1 = 3000$ K, $T_2 = 3200$ K and $T_3 = 3400$ K), which were attainable, since the melting temperature of the nanocrystals with Bazak potentials was approximately 3500 K. To obtain the mean square displacement, at each temperature, about 60 computational experiments were performed.

In Fig. 7, the resulting $\langle a^2(t) \rangle$ curve at $T = 3400$ K is presented. Similarly to the graph in Figure 3, the curve here has two sections. In the first section, interstitial diffusion is realized. The diffusion coefficient, which corresponds to this section according to Einstein relation (5), coincides almost precisely with the coefficient obtained without taking into account the trapping.

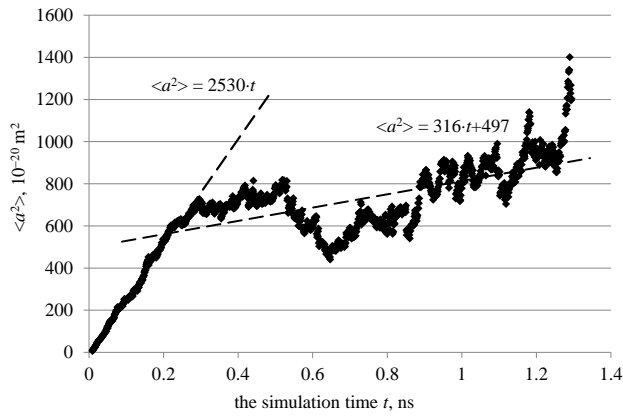


Fig. 7. The mean square displacement of xenon atoms including trapping in the uranium sites; Potentials II, $T = 3400$ K.

The slope of the second section of the graph in Fig. 8 characterizes the migration of the atoms that spend part of the time being captured in the uranium sites. The effective diffusion coefficient obtained for this slope from (5) has value $D_{\text{eff}} = 5.3 \cdot 10^{-6} \text{ cm}^2/\text{s}$.

Coefficient D_{eff} rapidly decreases with temperature, as it is shown in Fig. 8. On the interval of 400 K, the value of D_{eff} dropped by three orders of magnitude. The authors were able to obtain just three points of dependence $D_{\text{eff}}(T)$ in this work, however these points fit well on one straight line in the Arrhenius coordinates.

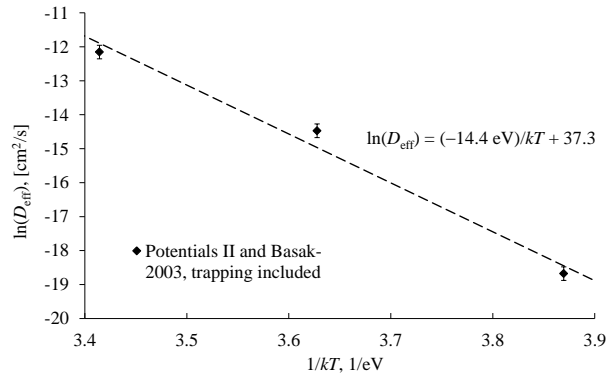


Fig. 8. Effective xenon diffusion coefficient $D_{\text{eff}}(T)$ obtained with allowance for the entrapment of the atoms by the uranium sites; Potentials II.

The graph in Fig. 8 is characterized by effective activation energy $E[D_{\text{eff}}, \text{II}] = (14 \pm 2) \text{ eV}$. The high magnitude of this energy can be explained if the potential diffusion barrier is formed as the sum of the energy required to move the atom from uranium vacancy into an interstitial position and the activation energy of interstitial migration.

The energies of solution of the Xe atom in the vacancy and the interstice for Potentials II coupled with Basak-2003 potentials were calculated in [10]. The minimum energy of the atom in the uranium vacancy corresponded to the configuration with two oxygen vacancies attached to it and amounted to 0.9 eV. The interstitial solution energy was equal to 9.62 eV. The summation of the difference between the two

values and the interstitial migration energy $E_{\text{D}}[\text{II}] = 2.2 \text{ eV}$ yields 10.9 eV as an estimate of $E[D_{\text{eff}}, \text{II}]$. The estimate is somewhat lower than 14 eV; however, it has the same order of magnitude. Taking into account the roughness of both estimates, the coincidence can be considered acceptable.

IV. THE RESULTS IN COMPARISON WITH THE EXPERIMENTAL DATA

The model nanocrystals in this work had stoichiometric composition $\text{UO}_{2+0.00}$. The experimental data on xenon bulk diffusion in such crystals exists for the temperatures below 2000 K [16]. Thus, a direct comparison of the results of the present work with experimental data is impossible. However, the experimental dependence of xenon diffusion coefficient $D_{\text{exp}}(T)$ in the Arrhenius coordinates is a straight line that can be extrapolated into the high temperature region as it is shown in Fig. 9.

An interesting result of the comparison is that the values of calculated interstitial diffusion coefficient $D_{\text{I}}(T)$ lie directly on the line that extrapolates the experimental data to higher temperatures. Unfortunately, dependence $D_{\text{I}}(T)$ is obtained in a too narrow temperature range, and so the degree of the coincidence cannot be determined on the basis of current simulation.

The coefficients of interstitial migration $D_{\text{II}}(T)$ obtained using Potentials II appear to be substantially underestimated with respect to the experimental data. The obtained estimate of the effective activation energy of diffusion that includes atom trapping in uranium sites $E[D_{\text{eff}}, \text{II}]$ does not correspond to the experiment either, where the observed activation energy is about 3.5 eV. It could be necessary to investigate more complex diffusion mechanisms to explain the experimental data.

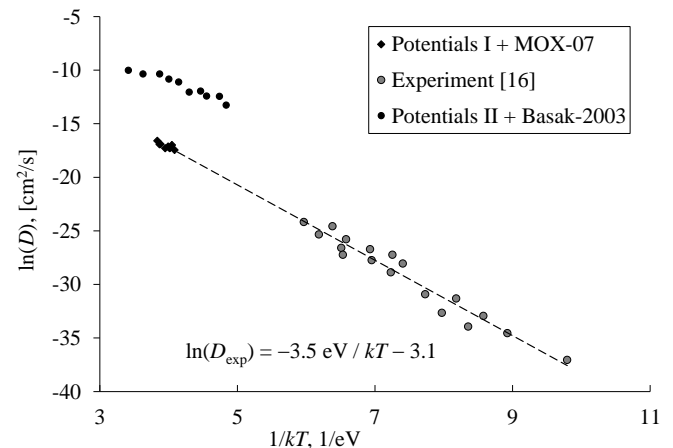


Fig. 9. Experimental data in comparison with the results of this work.

V. CONCLUSION

The following main results were obtained in this work:

1. Within the framework of molecular dynamics, the process of diffusion of individual xenon atoms in UO_2

nanocrystals of stoichiometric composition was studied. The nanocrystals had a free surface and were isolated in a vacuum.

2. Interstitial migration of the atoms was observed, as well as atom trapping in the sites of the uranium sublattice. The coefficients of interstitial diffusion and the characteristic times of release of xenon atoms from the cation vacancies varied by 2-3 orders of magnitude, depending on the choice of the potentials of interaction of Xe atoms with the environment.

3. The activation energies of interstitial xenon diffusion were obtained using potentials [4] and [10]. The values are, respectively, (2.5 ± 0.7) eV and (2.2 ± 0.2) eV in the temperature ranges of 2840–3025 K and 2400–3400 K.

4. For potentials [10], an estimate of the effective activation energy of xenon diffusion was obtained, taking into account the atom trapping in the uranium sites. This energy amounted to (14 ± 2) eV. A qualitative explanation of this estimate was proposed based on the static calculations carried out in [10].

5. The values of the coefficient of interstitial diffusion calculated with the use of potentials [4] fell on the straight line that extrapolates the experimental data to high temperatures. To clarify the meaning of this coincidence, additional research is needed.

Acknowledgment

The study was funded by the Russian Foundation for Basic Research (RFBR) according to research project No. 16-52-48008.

References

- [1] D.C. Parfitt and R.W. Grimes, "Predicting the probability for fission gas resolution into uranium dioxide," *J. Nucl. Mater.*, vol. 392, pp. 28–34, 2009.
- [2] K. Govers, C.L. Bishop, D.C. Parfitt, S.E. Lemehov, M. Verwerft and R.W. Grimes, "Molecular dynamics study of Xe bubble re-resolution in UO_2 ," *J. Nucl. Mater.*, vol. 420, pp. 282–290, 2012.
- [3] K. Govers, S.E. Lemehov and M. Verwerft, "Molecular dynamics study of grain boundary diffusion of fission gas in uranium dioxide," *Defect and Diffusion Forum*, vols. 323–325, pp. 215–220, 2012.
- [4] R. Jackson and C.R.A. Catlow, "Trapping and solution of fission Xe in UO_2 ," *J. Nucl. Mater.*, vol. 127, pp. 161–166, 1985.
- [5] P. Nerikar, T. Watanabe, J.S. Tulenko, S.R. Phillpot and S.B. Sinnott, "Energetics of intrinsic point defects in uranium dioxide from electronic-structure calculations," *J. Nucl. Mater.*, vol. 384, pp. 61–69, 2009.
- [6] G.E.P. Box and M.E. Muller, "A note on the generation of random normal deviates," *The Annals of Mathematical Statistics*, vol. 29, pp. 610–611, 1958.
- [7] H.J. C. Berendsen, J.P.M. Postma, W.F. van Gunsteren, A. DiNola and J.R. Haak, "Molecular-Dynamics with Coupling to an External Bath," *Journal of Chemical Physics*, vol. 81, pp. 3684–3690, 1984.
- [8] H.Y. Geng, Y. Chen, Y. Kaneta and M. Kinoshita, "Molecular dynamics study on planar clustering of xenon in UO_2 ," *Journal of Alloys and Compounds*, vol. 457, pp. 465–471, 2008.
- [9] A. Chartier, L. Van Brutzel and M. Freyss, "Atomistic study of stability of xenon nanoclusters in uranium oxide," *Phys. Rev. B*, vol. 81, pp. 174111-1–174111-9, 2010.
- [10] A.E. Thompson, B. Meredig and C. Wolverton, "An improved interatomic potential for xenon in UO_2 : a combined density functional theory/genetic algorithm approach," *J. Phys.: Condens. Matter*, vol. 26, pp. 105501-1–105501-9, 2014.
- [11] S.I. Potashnikov, A.S. Boyarchenkov, K.A. Nekrasov, A.Ya. Kupryazhkin, "High-precision molecular dynamics simulation of UO_2 - PuO_2 : Pair potentials comparison in UO_2 ," *J. Nucl. Mater.*, vol. 419, pp. 217–225, 2011.
- [12] S.I. Potashnikov, A.S. Boyarchenkov, K.A. Nekrasov, A.Ya. Kupryazhkin, "High-precision molecular dynamics simulation of UO_2 - PuO_2 : Anion self-diffusion in UO_2 ," *J. Nucl. Mater.*, vol. 433, pp. 215–226, 2013.
- [13] A.S. Boyarchenkov, S.I. Potashnikov, K.A. Nekrasov, A.Ya. Kupryazhkin, "Molecular dynamics simulation of UO_2 nanocrystals melting under isolated and periodic boundary conditions," *J. Nucl. Mater.*, vol. 427, pp. 311–322, 2012.
- [14] C.B. Basak, A.K. Sengupta, H.S. Kamath, "Classical molecular dynamics simulation of UO_2 to predict thermophysical properties," *Journal of Alloys and Compounds*, vol. 360, pp. 210–216, 2003.
- [15] P. M. Morse, "Diatomic molecules according to the wave mechanics. II. Vibrational levels," *Phys. Rev.*, vol. 34, pp. 57–64, 1929.
- [16] W. Mickleley, F. Felix, "Effect of stoichiometry on diffusion of xenon in UO_2 ," *J. Nucl. Mater.*, vol. 42, pp. 297–306, 1972.